

## Electronic structure of the ideal and reconstructed Si(001) surface\*

G. P. Kerker,<sup>†</sup> Steven G. Louie,<sup>‡</sup> and Marvin L. Cohen

*Department of Physics, University of California and Materials and Molecular Research Division,  
Lawrence Berkeley Laboratory, Berkeley, California 94720*

(Received 18 July 1977)

A self-consistent pseudopotential method is used to calculate the electronic structure of the (001) surface of Si. The results for the ideal  $1 \times 1$  surface are discussed in terms of density-of-states curves and charge-density distributions and compared with earlier calculations. The calculation for the reconstructed surface is based on the geometry recently obtained by Jona *et al.* using a low-energy-electron-diffraction (LEED) intensity analysis. It assumes that the surface reconstructs in a  $2 \times 1$  pattern by forming zig-zag chains along the [100] or [010] direction of the surface plane. Although this geometry agrees with observed LEED spectra far better than any of the previously discussed reconstructions, our calculation yields a metallic surface for this geometry. This results primarily from surface states which arise from broken bonds in the surface and the second atomic layer. In addition, the calculated local density of states near the surface is not consistent with existing photoemission data.

### I. INTRODUCTION

The atomic and electronic structure of the Si (001) surface has been the object of extensive experimental<sup>1-5</sup> and theoretical<sup>6-8</sup> investigation. A major problem is the fact that the atomic arrangement at this surface is not known. Low-energy-electron-diffraction (LEED) studies<sup>1,4</sup> of clean Si(001) surfaces reveal a  $2 \times 1$  reconstruction, that is a doubling of the periodicity along the [100] or [010] direction in the surface plane compared with a corresponding bulk plane.

A number of more or less plausible structural models have been proposed<sup>1,9-12</sup> for this reconstruction. Two of the simpler ones have been discussed extensively: One is the pairing model, the other is the vacancy model, both originally proposed by Schlier and Farnsworth.<sup>9</sup> Both models have been compared with each other on the basis of a self-consistent calculation of the electronic structure of the surface by Appelbaum *et al.*<sup>8</sup> Their results favor the pairing model over the vacancy model, since it gives better agreement with existing photoemission data; however, the surface has metallic character for both geometries, possibly giving rise to a charge-density-wave instability. Appelbaum *et al.*<sup>13</sup> argued that this instability might be the origin of a secondary reconstruction seen on Si(001).

Very recently, Jona *et al.*<sup>14</sup> proposed an entirely different structural model which they derived from a LEED intensity analysis. Some of the main features of this model were previously suggested by Seiwatz.<sup>15</sup> In particular, the surface atoms are assumed to form a zig-zag chain along the [100] or [010] direction of the surface plane. This so-called conjugated-chain model gives a much better correspondence with the observed LEED intensity

spectra than any other proposed reconstruction, including the vacancy and the pairing models.

In this paper the electronic structure of both the ideal  $1 \times 1$  Si (001) surface and the  $2 \times 1$  reconstructed surface is studied using a self-consistent pseudopotential method.<sup>16,17</sup> The geometry of the chain model is adopted for the reconstructed surface.

The paper is outlined as follows. In Sec. II we review the geometries of the Si (001) ideal and the chain-reconstructed surfaces. In Sec. III we briefly describe the calculational techniques. The results of our calculation are presented and discussed in Sec. IV for the ideal surface and in Sec. V for the reconstructed surface. In Sec. VI we summarize our results and present some conclusions.

### II. GEOMETRY OF THE IDEAL AND RECONSTRUCTED SURFACE

The atomic positions of the atoms in the topmost four layers of an ideal Si (001) surface are depicted in Fig. 1(a). The surface unit cell is a square containing one atom per cell with two broken bonds. The corresponding surface Brillouin zone (SBZ) is shown in Fig. 1(b) together with the labeling of various symmetry points. It can be seen from Fig. 1(a) that there are four symmetry operations which leave the crystal unchanged: the identity, a twofold rotation about an axis perpendicular to the surface through the center of the indicated unit cell, and two mirror planes normal to each other and to the surface. Thus the irreducible part of the SBZ consists of one-quarter of the zone.

Next consider the surface reconstructed according to the chain model [Fig. 2(a)]. The zig-zag chains run along the [010] direction (y direction) in the surface plane. Two neighboring chains are

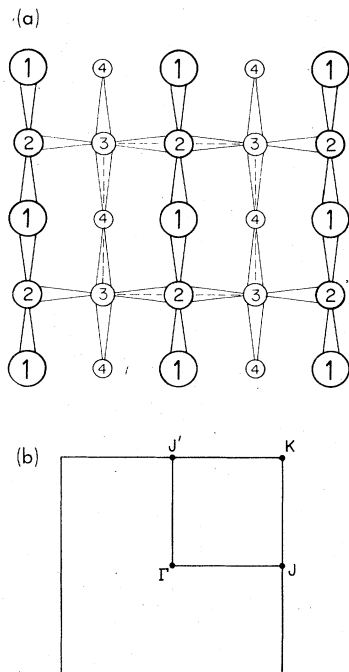


FIG. 1. (a) Orientation of the first four atomic layers of an ideal  $1 \times 1$  surface when viewed normal to the surface toward the bulk. The atoms are represented by circles. The number in a circle labels on atomic layer: "1" is the surface layer, "2" is the following second layer separated by  $\frac{1}{4}a$  where  $a = 5.43 \text{ \AA}$ , etc. The planar unit cell is a square of length  $a/\sqrt{2}$  indicated by the dashed lines. (b) The Brillouin zone corresponding to the planar unit cell of the ideal geometry.

separated along the  $[100]$  direction ( $x$  direction) by twice the nearest-neighbor distance of two atoms of the ideal surface, thus doubling the size of the surface unit cell in  $x$  direction.

The atoms in the second layer are shifted to make the back bond of each chain atom symmetrical with respect to the intrachain bonds. This arrangement roughly accounts for three of the four tetrahedral bonds of a chain and a second-layer atom: The intrachain bond angle is  $103^\circ$  and the angle between a chain bond and a back bond is  $101^\circ$ . There are two broken bonds per planar unit cell of the surface and second-layer plane introduced by this geometry, one associated with each chain atom pointing out of the paper plane in Fig. 2(a), and one associated with each second-layer atom directed toward an atom in the fifth layer. This point will come up again below. In addition to the reconstruction parallel to the surface, the second interlayer distance is contracted and has a value of  $1.22 \text{ \AA}$ , whereas all other interlayer distances are kept equal to the bulk-value  $1.36 \text{ \AA}$ .

From the structural parameters of this model

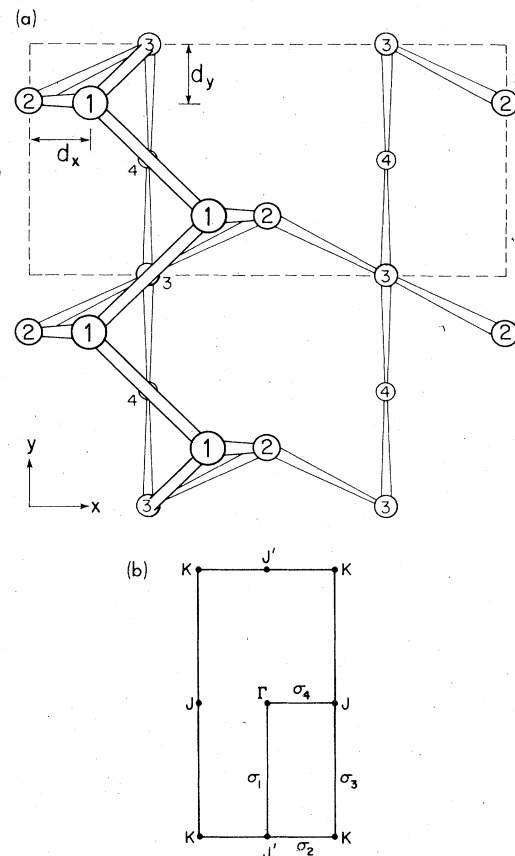


FIG. 2. (a) Orientation of the first four atomic layers of the  $2 \times 1$  reconstructed surface according to the chain model, viewed from the vacuum looking normally into the bulk. The symbols are the same as in Fig. 1(a). Layers 3 and 4 are displaced half a lattice vector along the  $y$  axis relative to Fig. 1(a). The planar reconstruction in the first two layers is characterized by the parameters  $d_x = 1.15 \text{ \AA}$  and  $d_y = 0.96 \text{ \AA}$ . The planar unit cell is a rectangle indicated by the dashed lines. (b) Brillouin zone of the  $2 \times 1$  planar unit cell with selected lines along which the energy bands are calculated. The area enclosed by these lines does not represent the irreducible part of the zone.

one obtains the following bond lengths: the distance between two nearest neighbors in the chain is  $2.45 \text{ \AA}$  (bulk value  $2.35 \text{ \AA}$ ), the back bond length of a chain atom is only  $1.8 \text{ \AA}$ , and the shortest distance between a second-layer and a third-layer atom is  $2.47 \text{ \AA}$ .

This model eliminates the two mirror planes present in the ideal case and leaves as symmetry operations of the crystal the identity and a twofold rotation about an axis perpendicular to the surface through the center of a chain bond. The irreducible part of the SBZ [Fig. 2(b)] is therefore one-half of the zone.

### III. CALCULATIONAL TECHNIQUES

To calculate the electronic structure for the two geometries we consider a 12-layer slab of Si with three layers of empty space added on top of a (001) surface on both sides. This arrangement is repeated periodically throughout the whole of space, permitting us to apply standard band-structure techniques to solve for the electronic structure of the surface on both sides of a film. For calculational convenience we introduce inversion symmetry into this "slab crystal," which means in the case of reconstruction that both surfaces of a slab are reconstructed. A slab surface still represents the "true" surface as long as the film of material and the vacuum between the slabs are thick enough to decouple the various slab surfaces. A detailed discussion of the method has been given in Refs. 16 and 17; therefore, it will only be briefly described below.

The inputs into the calculation include the atomic structure given in Sec. II and an ionic pseudopotential. In the case of Si, this potential may be expressed solely in terms of a local pseudopotential. This approach has been shown to give highly satisfactory results for both bulk and surface calculations on Si. For  $\text{Si}^{4+}$  the Fourier coefficients of the ionic pseudopotential may be obtained from

$$V_{\text{ion}}(q) = (a_1/q^2)[\cos(a_2q) + a_3]e^{a_4q^4}, \quad (1)$$

where the parameters  $a_i$  are given in Table I for both geometries. The ionic pseudopotential is screened by adding a Hartree potential  $V_H$  determined from Poisson's equation and an exchange potential  $V_x$  determined from the cube root of the charge density. The Fourier coefficients for  $V_H$  and  $V_x$  are given by

$$V_H(\vec{q}) = (4\pi e^2/\vec{q}^2)\rho(\vec{q}), \quad (2)$$

$$V_x(\vec{q}) = -\alpha(3/2\pi)(3\pi^2)^{1/3}e^2\rho^{1/3}(\vec{q}), \quad (3)$$

where  $\alpha = 0.79$  and  $\rho(\vec{q})$  and  $\rho^{1/3}(\vec{q})$  are the Fourier components of  $\rho(\vec{r})$  and  $\rho^{1/3}(\vec{r})$ , respectively.

The justification for using Slater's exchange potential and the choice of  $\alpha$  is discussed in detail in Refs. 16 and 17. Using a plane-wave expansion to diagonalize the Hamiltonian, the secular equation

TABLE I. Ionic pseudopotential parameters as defined in Eq. (1). The units are such that if  $q$  is entered in atomic units (a.u.), then  $V(q)$  is in Ry. The potentials are normalized to an atomic volume of 190 a.u.

$a_1$	0.813 71
$a_2$	0.790 65
$a_3$	-0.352 01
$a_4$	-0.018 07

may be written in the form

$$|H_{\vec{G}\vec{G}'}(\vec{k}) - E(\vec{k})\delta_{\vec{G}\vec{G}'}| = 0, \quad (4)$$

where  $\vec{G}$  denotes a reciprocal-lattice vector and

$$H_{\vec{G}\vec{G}'} = |\vec{k} + \vec{G}|^2 \delta_{\vec{G}\vec{G}'} + V_{\text{ion}}(|\vec{G} - \vec{G}'|)S(\vec{G} - \vec{G}') \\ + V_H(\vec{G} - \vec{G}') + V_x(\vec{G} - \vec{G}'). \quad (5)$$

The structure factor is denoted by  $S(\vec{G})$ .

Self-consistency was achieved by the following iteration process. The cycle is initiated by diagonalizing the Hamiltonian for four special  $\vec{k}$  points<sup>18</sup> using an empirical starting potential. Once the wave functions at these  $\vec{k}$  points are known, a valence charge density is calculated and used to determine  $V_H$  and  $V_x$  via Eqs. (2) and (3). Thus, a new screening potential is obtained and the whole process is repeated until the screening potential is converged within 0.01 Ry. At this stage the eigenvalues are normally stable to within 0.1 eV. Finally, the convergence was checked by calculating the screening potential from 36 sampling points in the irreducible part of the two-dimensional Brillouin zone of the ideal surface, and from 18 sampling points, respectively, for the reconstructed surface. In both cases, the potentials were equal to the potentials obtained by the special point scheme within less than 0.5% for the largest Fourier components.

In the diagonalization process, approximately 180 plane waves were used to expand the wave function for the ideal geometry including 320 additional plane waves by Löwdin's perturbation scheme to improve the energy convergence. For the reconstructed geometry at least 380 plane waves are required in the expansion with another 900 plane waves via perturbation theory to get satisfactory convergence. Increasing these numbers results in a negligible change of the energy eigenvalues by less than 0.01 eV. The change in the screening potential obtained by including more plane waves in the expansion is about 2% for the largest Fourier components of the potential.

### IV. RESULTS FOR THE IDEAL GEOMETRY

As mentioned in Sec. II, by forming an ideal Si (100) surface one has to break two bonds per surface atom. The electrons which previously participated in these bonds will tend to occupy surface-induced states which are localized at the surface and have energies in the gap between the valence and conduction bands, because they can no longer take full advantage of the attractive bonding potential between the atoms. Two surface bands are found in the gap whose dispersion is plotted in Fig. 3 along certain symmetry directions in the irreducible part of the SBZ according to the notation

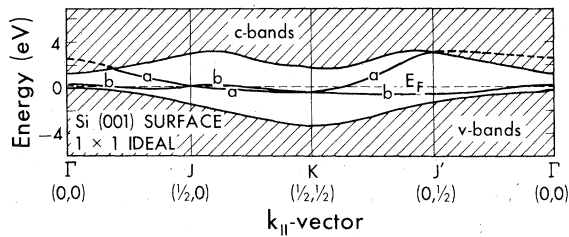


FIG. 3. Plot of the gap energy bands vs  $\vec{k}_{\parallel}$  for the ideal surface along symmetry lines in the SBZ. The continuum bulk energy levels (valence bands and conduction bands) are represented as striped regions. Where the  $a$  band merges into the conduction band and exists as a surface resonance, it is indicated by a dashed line. Energy is measured from the valence- and maximum. The Fermi energy  $E_F$ , given by a dashed line is found to have a value of 0.21 eV.

in Fig. 1(b). As discussed in Ref. 6, these two bands correspond to the symmetric and the antisymmetric combination of the two broken-bond orbitals. The band arising from the symmetric combination, denoted by  $b$  in Fig. 3, is generally lower in energy than the band associated with the antisymmetric combination, denoted by  $a$ , except along the symmetry line between  $J$  to  $K$ , where the  $a$  band lies slightly below (maximum = 0.2 eV) the  $b$  band. The  $a$  band merges into the conduction band along the symmetry line between  $J'$  and  $\Gamma$ , and along  $\Gamma$  and  $J$  near  $\Gamma$ . The bandwidth of the two bands is about 1 eV for the  $b$  band and about 3 eV for the  $a$  band. In Table II, we compare the energies of the two surface bands at  $\vec{k}_{\parallel} = \Gamma, J, K$ , and  $J'$  with the values of Ref. 6. Although our values differ from the energies quoted by Ref. 6 by 0.3–0.7 eV the overall behavior of the two surface bands along the chosen lines agrees reasonably well with the curves obtained by Ref. 6.

In Fig. 4(a) a charge-density contour map for a  $b$  band state at  $\vec{k}_{\parallel} = K$  is displayed. The plotting plane is perpendicular to the surface passing through a row of broken bonds. One finds a typical dangling bond state directed into the vacuum at a

TABLE II. Comparison of the surface band energies of the ideal surface at  $\vec{k}_{\parallel} = \Gamma, J, K$ , and  $J'$  obtained in this calculation (KLC) and by Appelbaum, Baraff, and Hamann (ABH). All energies are in eV and referenced to the valence-band maximum.

	$\Gamma$	$J$	$K$	$J'$	
$b$ band	0.352	0.204	-0.415	-0.312	KLC
	-0.02	-0.42	-1.13	-1.00	ABH
$a$ band	2.393	0.107	-0.322	2.89	KLC
	1.86	-0.50	-0.93	2.23	ABH

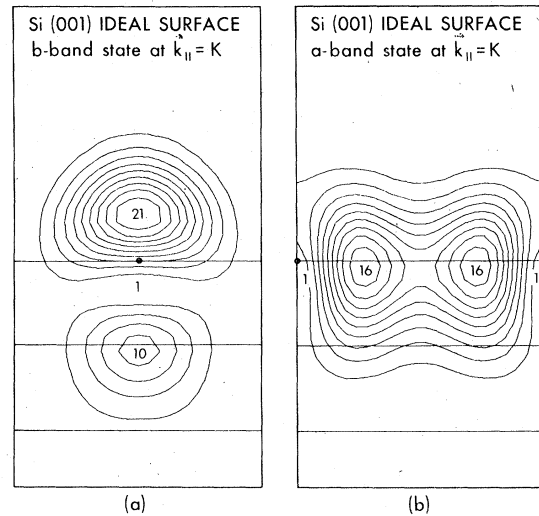


FIG. 4. Charge-density contour plots for two gap surface states at  $K$ . Atomic positions and atomic layers are indicated by dots and heavy lines, respectively. The plotting area starts in the vacuum and extends about  $3\frac{1}{2}$  atomic layers into the crystals passing through a row of broken bonds. Contours are normalized to one electron per unit cell. Successive contours are separated by one tenth of the maximum value of the charge density given in each plot.

right angle to the surface with a node just below the surface atom. Most of the charge (70%) is concentrated above the surface. The state decays very quickly into the bulk, the charge is practically confined to the first two surface layers.

In Fig. 4(b) the charge-density distribution of an  $a$  band state at  $\vec{k}_{\parallel} = K$  is plotted. The contour plane is the same as in Fig. 4(a). It is  $p_x$ -like and forms a kind of an electronic bridge between two surface atoms. It is even more localized at the surface than the corresponding  $b$ -band state. The larger width of this band stems from the overlap of the  $p_x$  orbitals and gives rise to an overlap in energy between the  $a$  band and  $b$  band, thus making the surface at least semimetallic. The redistribution of the electrons from the broken bonds has a considerable effect on the screening of the ionic potentials at the surface thus giving rise to back-bond surface states. These states are relatively weakly split from the bulk bands and mainly exist in the gap regions of the valence bands. A charge-density contour plot of a typical back-bond state found at  $K$  at an energy of -6.90 eV from the valence band edge is plotted in Fig. 5. The contour plane is normal to the surface and passes through a row of complete back bonds between atoms in the first and second layer. The state is highly localized below the surface atoms in the first interlayer region. An excellent overall picture of all the sur-

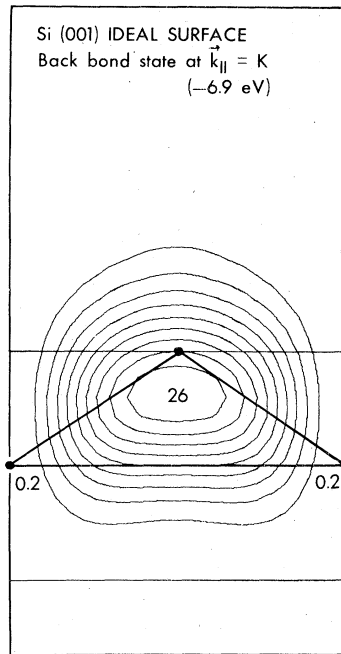


FIG. 5. Charge-density contour plot for a surface back-bond state at  $K$  around  $-6.9$  eV using the same conventions as in Fig. 4. The plotting area passes through a row of back bonds which are indicated by heavy lines joining the surface atom with the two atoms in the second atomic layer.

face states occurring in this model is obtained by calculating the local density of states (LDOS)

$$N_i(E) = \sum_{\vec{k}_{\parallel}, n} \int_{\Omega_i} |\psi_{\vec{k}_{\parallel}, n}(\vec{r})|^2 \delta(E - E_n(\vec{k}_{\parallel})) d^3r, \quad (6)$$

where  $\vec{k}_{\parallel}$  is the wave-vector parallel to the surface,  $n$  is the band index,  $\psi_{\vec{k}_{\parallel}, n}$  is the electronic wave function and  $\Omega_i$  is the integration volume of a region  $i$ .

We have calculated the LDOS for a thin slab, an interlayer spacing thick and centered around an innermost layer and around the surface layer, respectively, using 36 points in the irreducible part of the SBZ. The resulting histograms are displayed in Figs. 6(a) and 6(b). It can be seen from Fig. 6(a) that the LDOS in the interior of a Si slab strongly resembles the Si bulk density of states, whereas the surface LDOS in Fig. 6(b) has changed drastically reflecting the effect of the different surface geometry on the electronic states.

In the region of the absolute gap three peaks appear. The peak around 0 eV has less dispersion in energy, is therefore higher and is obviously associated with the  $b$ -surface band. The two smaller peaks between 0.5 and 2 eV are associated with  $a$ -band surface states. In fact, the two-peak structure of the upper surface band is due to the sta-

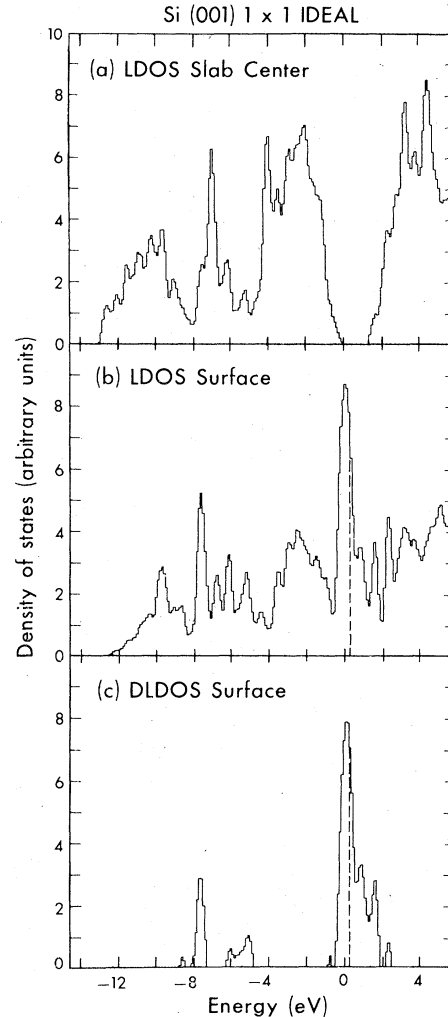


FIG. 6. Calculated local-density-of-states (LDOS) curves for the  $1 \times 1$  ideal surface. The difference curve of the local density of states (DLDOS) at the surface is discussed in the text.

tistics and should end up in a broad one-peak structure centered midgap, if one includes more  $\vec{k}$  points in the calculation of the density of states. In addition if one plots a difference curve by subtracting the LDOS at the center of the slab from the LDOS at the surface and keeps only the positive contributions the energy regions where back-bond surface states occur, are clearly revealed [Fig. 6(c)].

## V. RESULTS FOR THE RECONSTRUCTED GEOMETRY

Whereas the influence of the Si (100) ideal surface on the electronic structure is practically confined to the first two surface layers, the distortions from the tetrahedral bonding pattern introduced by the chain model, affect, as we will see

below, the electronic structure of the first four surface layers. Besides the planar reconstruction in the first two layers, the backward relaxation of the second layer toward the bulk creates a region between the second and third layer which has a slightly more attractive potential than the corresponding bulk region. We expect, therefore, an accumulation of charge between the second and third layer. Clearly, the very short back bond between a chain atom and a second-layer atom has a potential which is more attractive than anywhere else in the crystal and gives rise to surface states which, in fact, lie below the bottom of the valence band.

The four broken bonds per half slab unit cell are schematically depicted in Fig. 7. Note that the orbitals 1 and 2 do not lie in the same plane, but are twisted against each other, orbital 1 pointing into the vacuum and orbital 2 pointing toward the bulk into a region of relatively weak potential. The same holds for orbital 3 and 4 since these orbitals are obtained by rotating 1 and 2 by an angle  $\pi$  around the indicated axis. These orbitals, energetically very close to each other, combine linearly and give rise to four surface bands which lie in the absolute gap.

The combination from which these bands could be derived are

$$\begin{aligned}\phi_A &= \alpha_1(|1\rangle + |3\rangle) + \beta_1(|2\rangle + |4\rangle), \\ \phi_B &= \alpha_2(|1\rangle - |3\rangle) + \beta_2(|2\rangle - |4\rangle), \\ \phi_C &= \alpha_3(|1\rangle + |3\rangle) - \beta_3(|2\rangle + |4\rangle), \\ \phi_D &= \alpha_4(|1\rangle - |3\rangle) - \beta_4(|2\rangle - |4\rangle).\end{aligned}\quad (7)$$

The coefficients  $\alpha_i, \beta_j$  are a measure for the coupling between the surface and the second-layer orbitals.

The dispersion of the four bands along selected lines in the SBZ is shown in Fig. 8. The lowest completely occupied band, denoted by A, merges

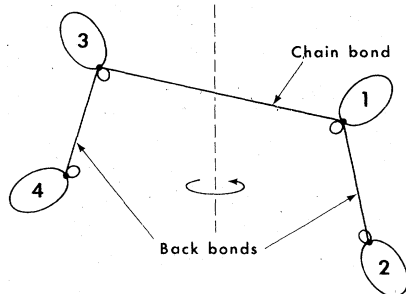


FIG. 7. Broken bonds introduced by the chain geometry. Orbitals 1 and 3 belong to chain atoms and are directed into the vacuum. Orbitals 2 and 4 belong to the second-layer atoms and point towards the bulk. Also indicated is the twofold rotation axis perpendicular to the surface.

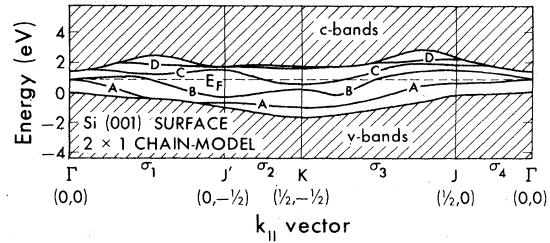


FIG. 8. Plot of the gap energy bands vs  $\vec{k}_{\parallel}$  for the  $2 \times 1$  reconstructed surface along selected lines in the SBZ.

into the valence band only along the  $\sigma_1$  line, whereas the uppermost completely unoccupied band, denoted by D, is more a surface resonance than a real surface band, since it is very close to or lies inside the conduction band. The Fermi energy  $E_F$  is indicated by a dashed line. We found a value of  $E_F = 0.9$  eV from using 36  $\vec{k}$  points throughout the

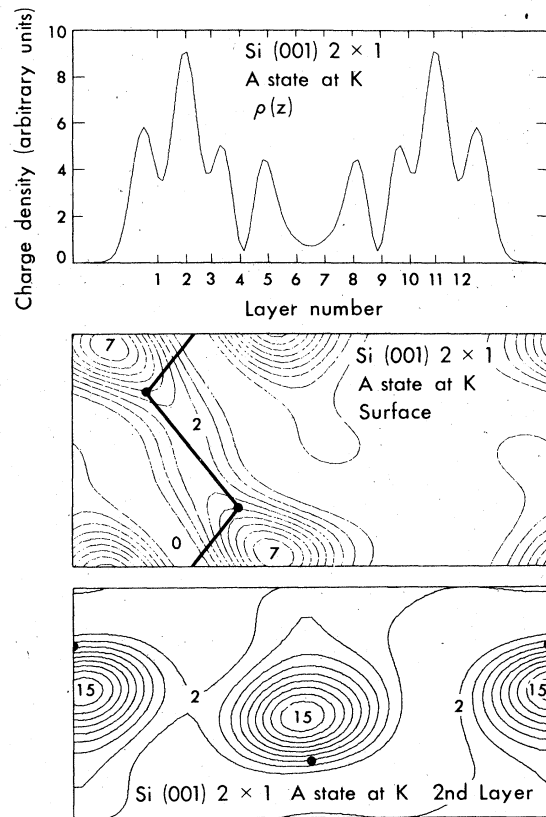


FIG. 9.  $x, y$ -integrated charge-density distribution along the  $z$  axis (perpendicular to the surface) and charge-density contour plots for a gap surface state of type A at K. The plotting areas are as indicated in the figures. The contours are normalized to one electron per unit cell. Successive contours are again separated by one-tenth of the maximum value of the charge density given in each plot.

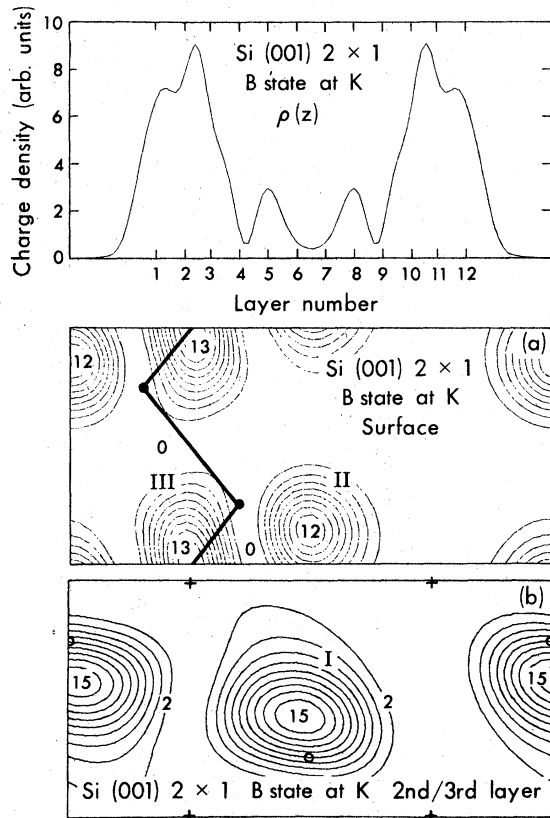


FIG. 10.  $x, y$ -integrated charge-density distribution along the  $z$  axis and charge-density contour plots for a gap surface state of type  $B$  at  $K$  using the conventions of Fig. 9. The contour plane of the bottom figure is parallel to the surface halfway between the second and third atomic layer. The atomic positions are indicated by open circles (second-layer atoms) and crosses (third-layer atoms).

whole SBZ. This value is relatively high compared to the experimental value of  $0.2 \pm 0.2$  eV given by Rowe.<sup>19</sup> We believe that this is due to the proposed geometry. The presence of two partially filled bands makes the surface, as in the ideal case, semimetallic.

It is difficult to display the charge density belonging to these bands in one contour plane in real space because of the distortions in this model.

In Fig. 9, the charge density integrated along the  $x, y$  directions is shown along an axis perpendicular to the surface for an  $A$  state at  $\vec{k}_{\parallel} = K$ . Most of the charge is concentrated around the second atomic layer, a charge-density contour map of this layer and the surface layer shows that this is a state derived from a linear combination of all four broken orbitals that leads to a maximum overlap. The states of  $B$  and  $C$  type which belong to the two partially filled bands, have again more charge in the vicinity of the second layer than at the surface

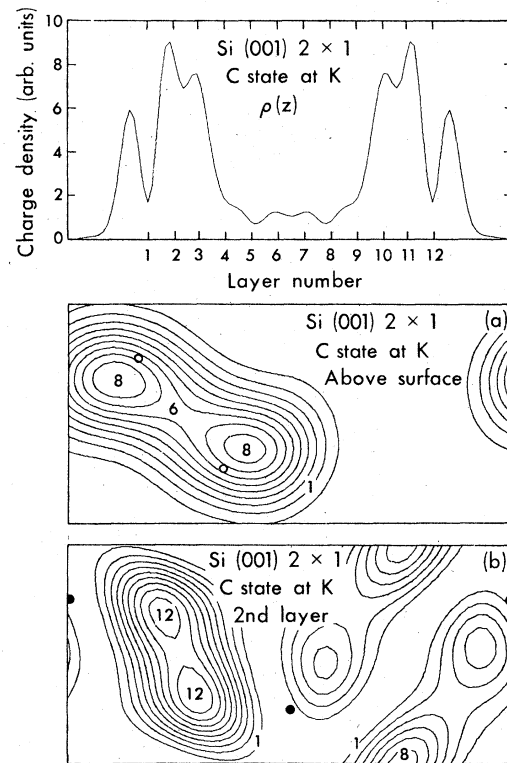


FIG. 11.  $x, y$ -integrated charge-density distribution along the  $z$  axis and charge-density contour plots for a gap surface state of type  $C$  at  $K$  using the conventions of Fig. 9. The open circles in the upper contour map refer to the positions of the atoms in the surface.

as can be seen from the  $x, y$ -integrated charge distributions along the  $z$  axis at  $\vec{k}_{\parallel} = K$  (Figs. 10 and 11).

The state of  $B$  type is generally lower in energy than the one of  $C$  type, the two broken orbitals along a chain back bond overlap, taking advantage of the attractive region along this bond direction. Various lobes of charge are found in the contour maps of the surface plane and a plane parallel to it halfway between the second and third atomic layer (Fig. 10). Lobe I is directed toward the third layer and contains most of the charge, lobe II is localized between the surface and the second layer, and lobe III has its maximum above the surface.

The  $C$ -type state consists of the symmetric combination of the two broken-bond orbitals in the same layer. Charge-density plots of a state at  $\vec{k}_{\parallel} = K$  are given in Fig. 11 in the second-layer plane and in a plane parallel to the surface halfway between the surface and a "vacuum plane." The  $D$ -type states arise from a combination of the broken orbitals with the smallest overlap. They are mainly localized above the surface (Fig. 12).

Up to now nothing has been said about the chain

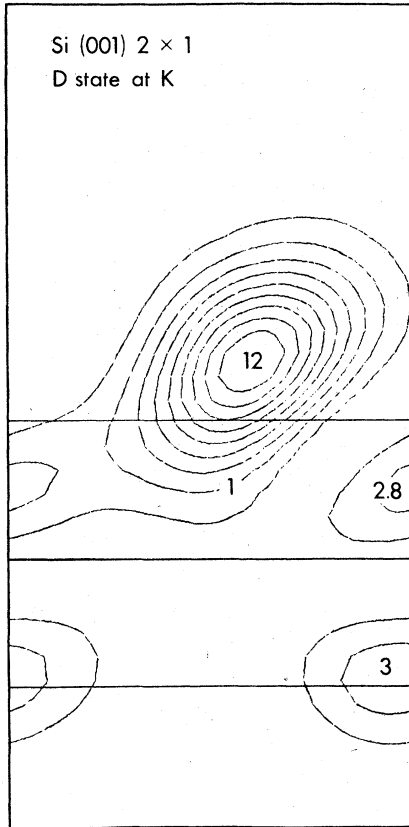


FIG. 12. Charge-density contour map of a gap surface state at  $K$  of type  $D$  using the conventions of Fig. 9. The plotting plane is perpendicular to the surface and parallel to the  $y$  axis passing through the center of the chain back bonds. It does not contain any atomic sites.

bonds and the back bonds between a chain-atom and a nearest neighbor atom in the second layer. Since these states can take full advantage of the attractive potential between the atoms which is very much bulklike or even stronger, the energy of these states is in the range of the valence band energies or lower. It should be noticed that both the chain bonds and the back bonds are split because of the effect of the potential of the third layer atom which makes one chain bond and one back-bond combination stronger than the other. The situation is illustrated in Figs. 13 and 14.

Various other states are found which are localized in the surface region, mainly between the second and third layer, arising from the distorted bonds between the atoms in these layers. These states are split away from the valence bulk states and exist in isolated gap pockets in the valence band region.

The energy distribution of all the surface states is exhibited in the LDOS histograms of Fig. 15.

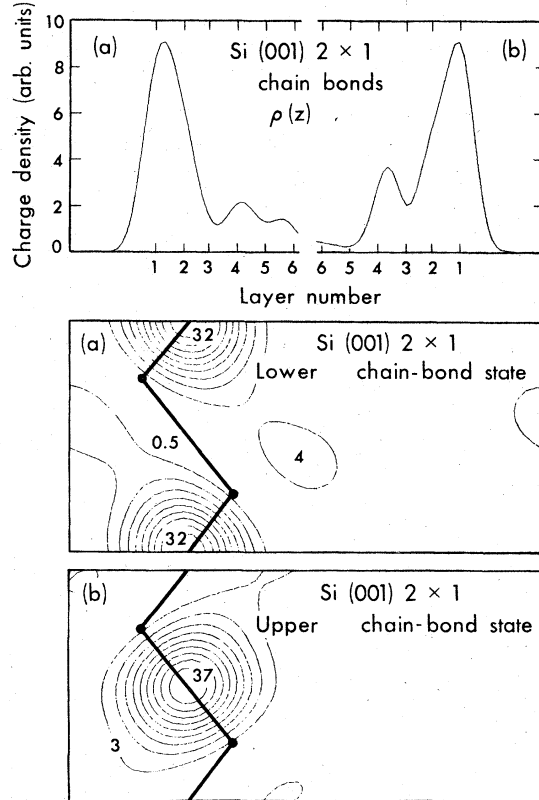


FIG. 13.  $x, y$ -integrated charge-density distribution along the  $z$  axis and charge-density contour plot for a lower (a) and an upper (b) chain-bond state at  $K$  using the conventions of Fig. 9. The contour plane is identical to the surface plane.

These histograms were obtained by using 18 points throughout the irreducible part of the SBZ. The uppermost diagram in Fig. 15 shows the LDOS within a layer in the center of a Si slab; it again resembles the Si bulk density of states fairly well, with slight differences because of the use of a smaller number of  $\vec{k}$  points and because of some influence of the surfaces. The histogram in the middle of Fig. 15 represents the LDOS within a small region around a surface layer. Subtracting the LDOS of the "bulk" layer from the surface LDOS and keeping only the positive contributions gives the third histogram of Fig. 15. This histogram reveals the energy distribution of the prominent surface states. There are roughly four regions, where states occur which are localized within the first four surface layers: Region  $A$  refers to the chain back-bond states, where obviously some of them lie below the bulk valence band; region  $B$  refers to states localized between the second and third layer, their contribution to the surface LDOS is therefore very small; region  $C$

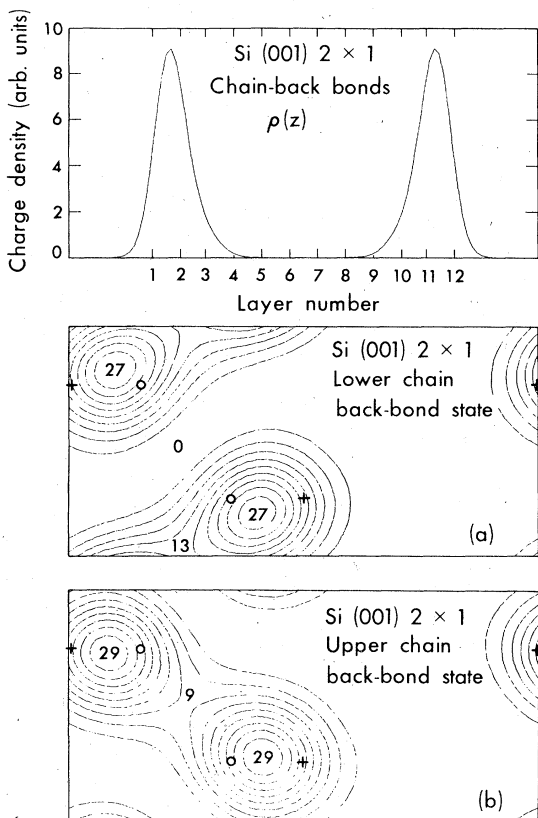


FIG. 14.  $x, y$ -integrated charge-density distribution along the  $z$  axis and charge-density contour plots for a lower and an upper chain back-bond state at  $K$  using the conventions of Fig. 9. The contour plane is parallel to the surface halfway between the surface and the second layer. The open circles mark the positions of the surface atoms, the crosses refer to the positions of the second-layer atoms.

refers to the chain bonds; and region  $D$ , which falls within the absolute gap, refers to the broken-bond surface states. The Fermi energy is indicated by a dashed line.

The shortcomings of the chain model are twofold. First, broken bonds are formed which are associated with atoms in different layers and which cannot take advantage of an attractive bonding potential. They give rise to surface states which lie in the energy gap between valence bands and conduction bands and overlap energetically, thus making the surface semimetallic. Second, the chain bond states occur at energies around  $-5$  eV below the bottom of the valence band edge (region  $C$ ) and cause a peak in the surface LDOS, whereas the corresponding photoemission spectrum shows a dip in this energy range (Fig. 15).

These results are quite insensitive to the unphysically short-chain back bond of the model used.

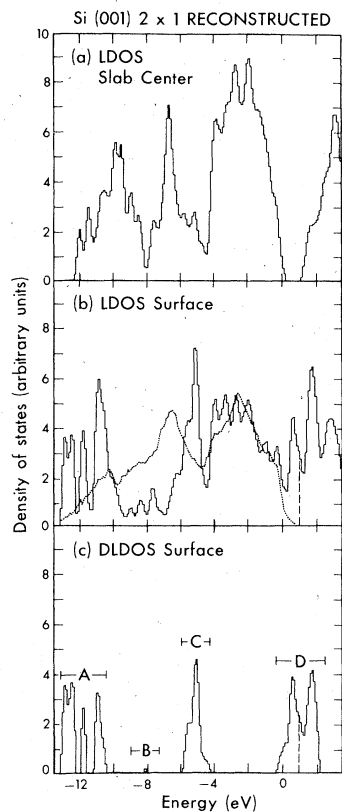


FIG. 15. Calculated LDOS curves for the  $2 \times 1$  reconstructed surface using the chain geometry. Also given in the surface LDOS histogram is the photoelectron density from Ref. 19. For the DLDOS at the surface see text. The regions  $A, B, C, D$  should not be confused with the surface band labels.

Jona *et al.*<sup>14</sup> proposed, as a modification of their model, to increase the first interlayer distance in order to stretch the chain back bond, and to further decrease the second interlayer distance to obtain a bulk length for the nearest-neighbor bonds between the second and third layer. This would actu-

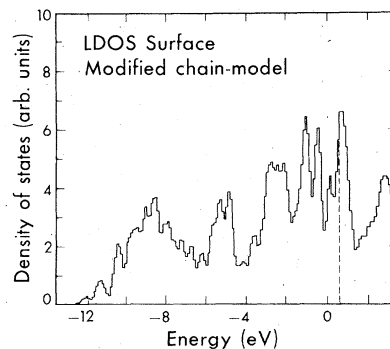


FIG. 16. Calculated LDOS curve at the surface of the modified chain model (see text).

ally bring the bulk closer to the second layer and provide more bonding potential for the second-layer broken bond; on the other hand, the surface layer would be more decoupled from the bulk with even less bonding strength for the surface broken bond. Furthermore, the splitting between the chain states should be smaller. Except for the chain back-bond states we therefore do not expect a dramatic change in the surface LDOS. In fact, a self-consistent calculation carried out for this modification again yields a semimetallic surface and a peak in the surface LDOS around  $-5$  eV, as can be seen from Fig. 16.

The disagreement between our calculated surface density of states and the experimental data is related to the basic geometrical feature of this model, namely, the formation of atomic zig-zag chains in the surface plane, and not to the overall assumed geometry. This can clearly be seen if one plots the charge density of the  $C$ -type states of Fig. 15 in real space. These states are fairly localized along the chains and look like the charge densities of Fig. 13. On the basis of our results on the electronic structure of this reconstruction, we believe that the actual geometry of a clean  $2 \times 1$  reconstructed Si (001) surface is still an open question.

## VI. CONCLUSIONS

A self-consistent pseudopotential method has been applied to the Si (001) surface both for the ideal and for a  $2 \times 1$  reconstructed configuration found from a recent LEED analysis by Jona *et al.*<sup>14</sup> In both cases metallic surfaces are obtained resulting from unsaturated broken bonds.

The results for the ideal surface are consistent with previous calculations by Appelbaum *et al.*<sup>6</sup> Additional back-bond states between the surface and the second atomic layer are found and a density-of-states analysis is presented.

Upon reconstruction a complete discussion of all the surface states is given in terms of charge-density plots and LDOS histograms. It is shown that the formation of atomic chains in the surface plane which characterizes the reconstruction leads to a LDOS near the surface which disagrees with photoemission experiments.

## ACKNOWLEDGMENTS

We would like to thank Dr. J. A. Appelbaum, Dr. D. R. Hamann, Dr. W. Pickett, and Dr. M. Schlüter for helpful discussions. Part of this work was done under the auspices of the U. S. ERDA.

\*Supported in part by NSF Grant No. DMR76-20647.

†Supported by a German Science Foundation fellowship.

‡Present address: IBM Research Laboratory, Yorktown Heights, New York, 10598.

<sup>1</sup>R. E. Schlier and H. E. Farnsworth, *J. Chem. Phys.* **30**, 917 (1959).

<sup>2</sup>J. J. Lauder and J. Morrison, *J. Chem. Phys.* **37**, 729 (1962); *J. Appl. Phys.* **33**, 2089 (1962).

<sup>3</sup>W. Mönch, *Adv. Solid State Phys.* **13**, 241 (1973).

<sup>4</sup>H. D. Shih, F. Jona, D. W. Jepsen, and P. M. Marcus, *Phys. Rev. Lett.* **37**, 1622 (1976), and references therein.

<sup>5</sup>A. Ignatiev, F. Jona, M. Debe, D. E. Johnson, S. J. White, and D. P. Woodruff, *J. Phys. C* **10**, 1109 (1977).

<sup>6</sup>J. A. Appelbaum, G. A. Baraff, and D. R. Hamann, *Phys. Rev. B* **11**, 3822 (1975); *Phys. Rev. B* **12**, 5749 (1975).

<sup>7</sup>I. B. Ortenburger, S. Ciraci, and I. P. Batra, *J. Phys. C* **9**, 4185 (1976).

<sup>8</sup>J. A. Appelbaum, G. A. Baraff, and D. R. Hamann,

*Phys. Rev. B* **14**, 588 (1976).

<sup>9</sup>R. E. Schlier and H. C. Farnsworth, in *Semiconductor Surface Physics* (University of Pennsylvania, Philadelphia, 1959), pp. 3-22.

<sup>10</sup>J. Levine, *Surf. Sci.* **34**, 90 (1973).

<sup>11</sup>J. C. Phillips, *Surf. Sci.* **40**, 459 (1973).

<sup>12</sup>W. A. Harrison, *Surf. Sci.* **55**, 1 (1976).

<sup>13</sup>J. A. Appelbaum, G. A. Baraff, and D. R. Hamann, *Phys. Rev. B* **15**, 2408 (1977).

<sup>14</sup>F. Jona, H. D. Shih, A. Ignatiev, D. W. Jepsen, and P. M. Marcus, *J. Phys. C* **10**, L67 (1977).

<sup>15</sup>R. Seiwatz, *Surf. Sci.* **2**, 473 (1964).

<sup>16</sup>M. Schlüter, J. R. Chelikowsky, S. G. Louie, and M. L. Cohen, *Phys. Rev. Lett.* **34**, 1385 (1975); *Phys. Rev. B* **12**, 4200 (1975).

<sup>17</sup>S. G. Louie and M. L. Cohen, *Phys. Rev. Lett.* **35**, 866 (1975); *Phys. Rev. B* **13**, 2461 (1976).

<sup>18</sup>S. L. Cunningham, *Phys. Rev. B* **10**, 4988 (1974).

<sup>19</sup>J. E. Rowe, *Phys. Lett. A* **46**, 400 (1974).